THE JOURNAL OF PHYSICAL CHEMISTRY C

Article

pubs.acs.org/JPCC

Importance of the Reorganization Energy Barrier in Computational Design of Porphyrin-Based Solar Cells with Cobalt-Based Redox Mediators

Kristian B. Ørnsø,[†] Elvar Ö. Jónsson,[†,‡] Karsten W. Jacobsen,[†] and Kristian S. Thygesen*[,†]

[†]Center for Atomic-scale Materials Design, Department of Physics, Technical University of Denmark, Fysikvej, 2800 Kongens Lyngby, Denmark

Supporting Information

ABSTRACT: The shift from iodide-based redox mediators in dye-sensitized solar cells toward octahedral cobalt complexes has led to a significant increase in the efficiency. However, due to the nature of this type of complexes the driving force required for the regeneration of the dye is very high, and this limits the achievable efficiency. Here we show that the large driving force is a direct consequence of the large reorganization energy of the dye regeneration reaction. The reorganization energies for charge transfer between a simple zinc porphyrin dye and two popular cobalt-based redox mediators is calculated using ab initio molecular dynamics with explicit solvent. These results are then combined with a Marcus-based extrapolation scheme to obtain the reorganization energies of more than 5000 porphyrin-based dyes. We propose a scheme for scoring the performance of the porphyrin dyes, which is able to identify already known high-performance dyes in addition to a number of even better candidates. Our analysis shows that the large internal reorganization energy of the Co-based redox mediators is an obstacle for achieving higher efficiencies.

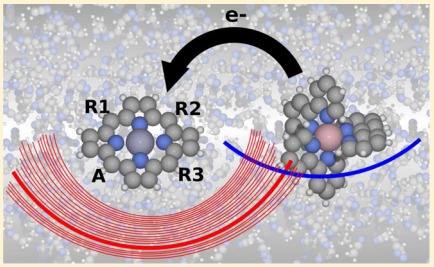

INTRODUCTION

As the search for sustainable energy sources is intensified, focus is put on exploiting the vast energy in sunlight. For this purpose, dye-sensitized solar cells (DSSC)[1] have since the emergence of the first efficient system in 1991[2] been considered promising candidates. In particular, the low material cost, flexibility, and high efficiency under low illumination conditions[3] of DSSCs make these stand out from the conventional semiconductor-based solar cells. In a standard DSSC the photons are absorbed by a molecule with a high absorption in the visible part of the solar spectrum. This creates a photoexicted electron in the dye which is transferred to the conduction band of a semiconductor nanoparticle (usually TiO_2) on which the dye is anchored. Following this, the electron is extracted to an external circuit and reintroduced into the cell via a counter electrode (usually Pt). In the last two steps, the electron is transferred from the counter electrode to a redox mediator and then from the redox mediator back to the dye completing the circuit. To improve the efficiency of DSSCs, much focus has been put on choosing the correct dye. Here, several factors are important including the correct level alignment of the dye orbitals with the semiconductor conduction band and the redox potential of the redox mediator, a large overlap between the dye absorption spectrum and the solar spectrum, the charge injection from the dye to the semiconductor, the regeneration of the oxidized dye by the redox mediator, losses due to charge transport and recombination, etc. More recently, functionalized porphyrins have gained interest as dyes in DSSCs due to their high absorption of visible light and high customizability.[4−13] The highest efficiencies obtained for DSSCs of 12.3%[14] and 13.0%[15] have both been obtained using porphyrin-based dyes. We previously reported a computational screening study of porphyrin-based dyes,[16,17] in which we investigated the effect of changing side and anchor groups for a range of different porphyrin backbones. In these studies we scored the dyes by computing a level alignment quality based only on the level alignment between the dye orbitals and the conduction band of TiO_2, while the redox potential of the redox mediator was treated as a simple variable. However, the reorganization energy associated with the electron transfer from the redox mediator to the oxidized dye is also an essential component to obtain a high DSSC efficiency. To include this effect in the level alignment quality, we here present a computational study in which we apply Marcus theory[18−22] to evaluate the solvent reorganization barrier for the regeneration reactions of functionalized porphyrins by two cobalt-based redox mediators. The cobalt-based redox mediators are chosen here since they are presently considered the most promising redox molecules[14,23] and the electron transfer is believed to be a simple outer-sphere process.

A schematic overview of the energetics associated with the regeneration reaction is given in Figure 1 (left). The regeneration process itself is defined as the electron transfer from a cobalt-based redox mediator to the oxidized dye

$$D^+ + [Co(red)]^{2+} \rightarrow D + [Co(red)]^{3+} \quad (1)$$

Received: December 18, 2014
Revised: March 24, 2015
Published: May 12, 2015

DOI: 10.1021/jp512627e
J. Phys. Chem. C 2015, 119, 12792−12800

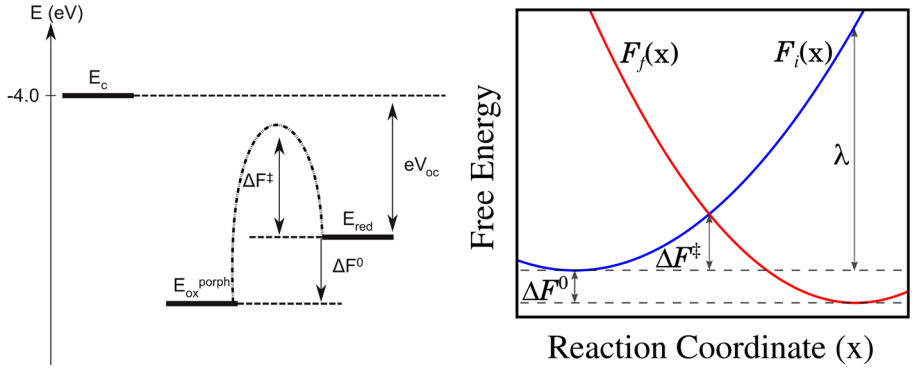

Figure 1. (Left) Scheme of the energetics associated with the regeneration reaction. Here, E_c is the conduction band edge of TiO_2, E_{ox}^{porph} is the oxidation potential of the porphyrin-based dyes, E_{red} is the redox potential of the cobalt-based redox mediator, ΔF^0 is the driving force for the regeneration reaction, $\Delta F^{\ddagger}$ is the barrier associated with the electron transfer, and eV_{oc} is the open-circuit voltage multiplied with the electronic charge. (Right) Schematic illustration of the free energy function for the initial, $F_i(x)$, and final, $F_f(x)$, electronic states. The reaction coordinate, $x = \Delta E(R^N)$ (see eq 3), is the vertical energy gap between the two electronic configurations corresponding to the left- and right-hand sides of eq 1. The gap collectively represents all fluctuations of the nuclear degrees of freedom of both the solute and the solvent environment, R^N. Running MD based solely on the initial and final electronic states gives information for their respective equilibrium values (the region around the minimum of the two curves). To achieve sampling in the intermediate region where the free energy barrier is defined our MD is based on the coupling parameter scheme (eq 6). Knowing one function the free energy change, barrier, and reorganization energy relative to the initial state can readily be solved for $\Delta F^0 = F_f(x_{f,min}) - F_i(x_{i,min})$, $\Delta F^{\ddagger} = F_i(x^{\ddagger}) - F_i(x_{i,min})$ and $\lambda = F_i(x_{f,min}) - F_i(x_{i,min})$, respectively. Here, $x^{\ddagger}$ and $x_{j,min}$ denote the reaction coordinate value at the crossing and minimum of the free energy functions. The parabolas presented here are an idealized case, which is realized under certain conditions, namely, linear response (see eq 14 and the section on Marcus Theory).

where D/D^+ is the neutral/oxidized dye and $[Co(red)]^{2+}/[Co(red)]^{3+}$ is the reduced/oxidized cobalt-based redox mediator. In Marcus theory the charge transfer rate between two species is expressed in terms of a pre-exponential factor (taking into account the donor−acceptor electronic state overlap factor) and an exponential term which accounts for the thermodynamic free energy that must be overcome to facilitate electron transfer. The latter term includes the redox potentials as well as the nuclear and electronic response of the solvent and solute to the transferred electron.

In this study we focus only on the exponential term in the Marcus rate expression from which we explicitly calculate the barrier for the smallest porphyrin dye. We then introduce a Marcus-based extrapolation scheme to estimate the barrier for more than 5000 porphyrin dyes present in our database.[16,17] In this way we combine large-scale computational screening with a more in-depth study of the simplest zinc porphyrin (ZnP) to improve the scoring of the dyes by introducing a correction term to the level alignment quality and at the same time identify parameters acting as obstacles for improving the efficiency of DSSCs.

METHODS

We used density functional theory (DFT)-based molecular dynamics (MD) calculations in combination with Marcus theory to calculate the solvent barrier associated with the regeneration (see eq 1) of unsubstituted zinc porphyrin by two different cobalt-based redox mediators. These calculations are extrapolated using a continuum model for the reorganization energy for more than 5000 functionalized porphyrins to provide an estimate of the overpotential related to the regeneration process. The two cobalt redox mediators investigated are the commonly used $[Co^{II/III}(bpy)_3]$ and $[Co^{II/III}(bpy\text{-}pz)_2]$ (bpy-pz = 6-(1*H*-pyrazol-1-yl)-2,2′-bipyridine).[23,24] The chemical structures of the two redox mediators and the functionalized porphyrin dyes are shown in Figure 2. In the figure for the porphyrin the R1, R2, and R3 labels denote side group locations, A denotes the anchor group location, and

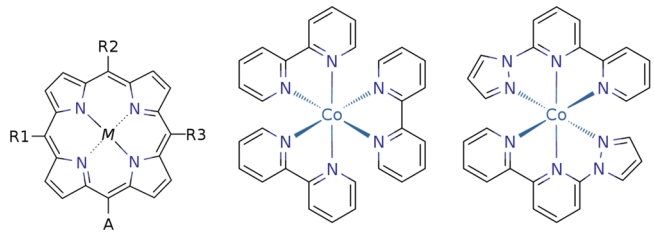

Figure 2. Molecules investigated in this work. (Left) Functionalized porphyrin dye with side groups (R1−R3) and acceptor group (A). (Middle) $[Co^{II/III}(bpy)_3]$ redox mediator. (Right) $[Co^{II/III}(bpy\text{-}pz)_2]$ redox mediator.

M denotes the metal center. The different metal centers, side, and anchor groups used in this study are described in detail in recent publications[16,17] and shown in Figures S2−S4, Supporting Information. In the following we briefly introduce the methods used in this study.

Free Energy Function. In order to address the free energy barrier we use the free energy function, defined by the restricted partition function of the vertical (potential) energy gap between the initial and the final state[25]

$$F_i(x) = -\frac{1}{\beta}\ln\int dR^N \delta(x - \Delta E(R^N)) e^{-\beta E_i(R^N)} = -\frac{1}{\beta}\ln[P_i(x)] + F_i^* \quad (2)$$

where the gap $\Delta E(R^N)$ is given by

$$\Delta E(R^N) = E_i(R^N) - E_f(R^N) \quad (3)$$

and i and f refer to the initial and final electronic states (i.e., left- and right-hand side of eq 1)

$$E_i = E[D^+ + [Co(red)]^{2+}]$$

$$E_f = E[D + [Co(red)]^{3+}]$$

DOI: 10.1021/jp512627e
J. Phys. Chem. C 2015, 119, 12792−12800

$P_i(x)$ denotes the probability distribution of the reaction coordinate, $x = \Delta E(R^N)$, for the initial state

$$P_i(x) = \frac{\int dR^N \delta(x - \Delta E(R^N)) e^{-\beta E_i(R^N)}}{\int dR^N e^{-\beta E_i(R^N)}} \quad (4)$$

Finally, F_i^* denotes the (absolute) free energy of the initial state. This quantity is not well defined; however, the expressions above completely define relative differences of the free energy function of the initial and final state. For example, rearranging eq 3 to $E_i(R^N) - \Delta E(R^N) = E_f(R^N)$ and inserting into the analogous expression for $F_f(x)$ one can show that $F_f(x) = F_i(x) - x$ (see Derivation 1, Supporting Information). In particular, the reorganization energy and free energy barrier can be determined from just one of the free energy curves (see Figure 1).

Sampling and Optimization. An accurate treatment of the integral expressions above requires knowledge of both equilibrium and nonequilibrium configurations, relevant for both the initial and the final electronic states. To achieve a proper sampling in the crossing region one defines intermediate states, α, as

$$\begin{aligned} E_\alpha(R^N) &= (1 - \chi_\alpha) E_i(R^N) + \chi_\alpha E_f(R^N) \\ &= E_i(R^N) - \chi_\alpha \Delta E(R^N) \end{aligned} \quad (5)$$

which connects the two states in a straightforward manner. The MD sampling of the relevant phase spaces are then based on a simple linear combination of the forces

$$\mathbf{F}_\alpha(R^N) = (1 - \chi_\alpha)\mathbf{F}_i(R^N) + \chi_\alpha \mathbf{F}_f(R^N) \quad (6)$$

where $\mathbf{F}_i$ and $\mathbf{F}_f$ are the force vectors for the initial and final states, respectively. The coupling parameter $\{\chi_\alpha : 0 \leq \chi_\alpha \leq 1\}$ is sampled at equally spaced intervals between 0 and 1, which obviously brings the system from the initial electronic charge state to the final electronic charge state. This ensures sampling of R^N in and out of equilibrium for either state, giving information for the free energy functions in the intermediate region, which is important for an accurate estimate of the free energy barrier, $\Delta F^{\ddagger}$ (see Figure 1). Note that the MD sampling employed here is further enhanced by constraining high-frequency degrees of freedom (hydrogen bonds) to allow for larger time steps when solving for the equations of motion. R^N, in all expression, denotes the active degrees of freedom present in the simulations which means that the Boltzmann factor, $\beta = (1/(k_B T))$, is scaled accordingly.

Employing the coupling parameter method as outlined above produces biased probabilities, $P_\alpha^b(\Delta E(R^N))$, which need to be corrected for the bias $-\chi_\alpha \Delta E(R^N)$, and subsequently combined to give the total probability curve for the initial state. To this end we use the weighted histogram analysis method (WHAM)[26−28] following the formulation of Souaille and Roux.[26]

In WHAM the unbiased probability is given by

$$P_\alpha^u(\Delta E(R^N)) = e^{\beta[-\chi_\alpha \Delta E(R^N) - f_\alpha]} P_\alpha^b(\Delta E(R^N)) \quad (7)$$

where f_α corresponds to the free energy change in the system due to the bias $-\chi_\alpha \Delta E(R^N)$ and is determined in a self-consistent fashion. The sampling is performed for N_α values of α, so the total probability curve for the initial state is written as

$$P_i(\Delta E(R^N)) = C \sum_{\alpha=1}^{N_\alpha} p_\alpha(\Delta E(R^N)) P_\alpha^u(\Delta E(R^N)) \quad (8)$$

where C is a normalization constant and $p_\alpha(\Delta E(R^N))$ are the weights of the sampling windows for a given value of the vertical potential energy gap $\Delta E(R^N)$. Now, requiring the weights to be normalized and minimize the statistical error in the sampling results in[26,27]

$$P_i(\Delta E(R^N)) = C \sum_{\alpha=1}^{N_\alpha} \frac{n_\alpha}{\sum_{\kappa=1}^{N_\alpha} n_\kappa e^{-\beta[-\chi_\kappa \Delta E(R^N) - f_\kappa]}} P_\alpha^b(\Delta E(R^N)) \quad (9)$$

where n_α is the number of samples in the window α. The unknown free energy change due to the bias can be solved in a self-consistent manner using

$$e^{-\beta f_\nu} = C \int dR^N \sum_{\alpha=1}^{N_\alpha} \frac{n_\alpha e^{-\beta[-\chi_\alpha \Delta E(R^N)]}}{\sum_{\kappa=1}^{N_\alpha} e^{-\beta[-\chi_\kappa \Delta E(R^N) - f_\kappa]}} P_\alpha^b(\Delta E(R^N)) \quad (10)$$

The expression above is solved using all available data points and is the most time-consuming step in the WHAM procedure, both because of the shear number of data points as well as strict convergence criteria. Furthermore, subtracting the value corresponding to the initial state, f_i, from all f_α ensures that eq 9 is normalized (C). As a last step we also introduce the normalized histograms into eq 9 to give a manageable number of data points for the construction and fitting of the free energy function (eq 2).

$$P_\alpha^b(x) = \frac{1}{n_\alpha} \sum_{l=1}^{n_\alpha} \delta(x - \Delta E(R_{\alpha,l}^N)) \quad (11)$$

Marcus Theory. In Marcus theory it is customary to split the total reorganization energy into internal and outer contributions

$$\lambda = \lambda^{in} + \lambda^{out} \quad (12)$$

The internal reorganization energy can be approximated as the energy difference of the solute species in the initial electronic state evaluated at the relaxed structures corresponding to the initial and final electronic states in vacuum. The outer reorganization energy is associated with the solvent structural response to the change in electronic charge on the solute species. This term was recognized by Marcus as the key factor in determining the rate of outer-sphere electron charge transfer reactions.[18−22]

In terms of a continuum model representing the solvent surrounding two solute species A and D represented as charged spheres of radius r_A and r_D, respectively, the outer reorganization energy in atomic units can be expressed as[18]

$$\lambda^{out} = (\Delta q^2)\left(\frac{1}{\epsilon^\infty} - \frac{1}{\epsilon^{st}}\right)\left(\frac{1}{2r_A} + \frac{1}{2r_D} - \frac{1}{R_{AD}}\right) \quad (13)$$

where ϵ^∞ and ϵ^{st} are the high-frequency and static dielectric constants of the solvent and Δq the total charge transferred. The last term on the right-hand side is the screened Coulomb interaction between the donor and the acceptor, where R_{AD} is the distance between the two solute species. Assuming that the charge transfer occurs when the two spheres come in contact R_{AD} is simply given by the sum of two solute species radii.

DOI: 10.1021/jp512627e
J. Phys. Chem. C 2015, 119, 12792−12800

In the linear response regime the sampled vertical energy gaps in the N_α windows display Gaussian statistics, with a relative shift of the mean value directly proportional to the coupling value α.[25,29] Under these conditions the free energy function reduces to a parabola[25,30]

$$F_i(x) = \frac{1}{4\lambda}(x - x_{\min,i})^2 + F_i^* \tag{14}$$

where $x_{\min,i}$ denotes the reaction coordinate associated with the equilibrium configurations of the initial state.

We do not explicitly calculate the reorganization energy of the reaction in eq 1 but split the reaction into two parts

$$D^+ + D \rightarrow D + D^+$$

$$[Co(red)]^{2+} + [Co(red)]^{3+} \rightarrow [Co(red)]^{3+} + [Co(red)]^{2+}$$

which in turn provides us with symmetric free energy curves after solving for the probability curves following the procedure in the preceding section (see Figures S5−S7, Supporting Information). The fully simulated free energy functions are fitted with a parabolic expression (it is easy to show that for this case $F_f(x) = F_i(x) - x$, see Derivation 2, Supporting Information). This in turn gives us the reorganization energy for the individual species which are then combined to give the reorganization energy for the total reaction in eq 1 (see the next section and eq 19).

Extrapolated Barrier Calculations. Due to limited computational resources it has been necessary to only explicitly calculate the reorganization energy for the simplest zinc porphyrin and extrapolate this value to the functionalized porphyrins. Functionalizing porphyrins significantly changes the size of the dye, and to account for this change we used the *Jmol* program suite[31] to obtain a volume of all 5000+ porphyrin dyes using the predefined van der Waals surfaces of the atoms. This volume is then transformed into a radius of a sphere using

$$r = \left(\frac{3V}{4\pi}\right)^{1/3} \tag{15}$$

Having this radius we can use a modified version of eq 13 in which we include a correction for using a finite cell with periodic boundary conditions to obtain the correlation between our chosen convention for r and the explicitly calculated reorganization energy for the simplest zinc porphyrin (see Table S1, Supporting Information)[32−34]

$$\lambda_{PBC}^{out} = (\Delta q)^2 c\left(\frac{1}{2r} + \frac{1}{2L_c}\left(\xi_{Ew} + \frac{4\pi}{3}\left(\frac{r}{L_c}\right)^2 - \frac{16\pi^2}{45}\left(\frac{r}{L_c}\right)^5\right)\right) \tag{16}$$

where λ_{PBC}^{out} is the uncorrected reorganization energy obtained from our MD simulation, L_c is the linearized cell length, $L_c = V^{1/3}$, where V is the volume of the cell, and ξ_{Ew} is the Madelung constant, which for our cell is $\xi_{Ew} = -2.757$. From the above equation we can estimate $c = (1/\epsilon^{\infty}) - (1/\epsilon^{st})$. This fitting was tested for both the "flat" zinc porphyrin species as well as the octahedral $Co(bpy)_3$ species, giving $c = 0.502$ and 0.520, respectively. These values are in good agreement with the inverse of the experimental dielectric constant of acetonitrile, $c \approx 0.53$. Our smaller values reflect an overestimated dielectric response, which PBE is known to do, e.g., for water. For the extrapolation scheme of the zinc porphyrin-based dyes $c = 0.502$ was used throughout.

Having corrected for the finite cell with periodic boundary conditions, we can define the r-dependent outer reorganization energy for the functionalized porphyrins as

$$\lambda_{porph}^{out}(r) = (\Delta q)^2 c\frac{1}{2r} \tag{17}$$

We again note that converting the volumes of porphyrins into spheres is a simplification. Apart from the usually flat structure of porphyrins, the way the dye is connected to the surface further influences the actual radius and accessible surface area of the dye as well as the distance to the redox complex.[35] However, since this approximation only enters the correction to an explicitly computed reorganization energy, we believe that we will obtain the correct trends in the size dependency.

To account for the screened coulomb interaction between the acceptor and the donor we apply a correction based on the $1/R_{AD}$ part of eq 13. Assuming that the electron transfer occurs when the acceptor and donor are right next to each other corresponds to setting $R_{AD} = r + r_{red}$, where r is still the dye radius and r_{red} is the radius of the redox mediator. Using this we obtain a correction to the outer reorganization given by

$$\lambda_R^{out}(r) = -(\Delta q)^2 c\frac{1}{r + r_{red}} \tag{18}$$

Having the size-dependent part of the reorganization energy and the corrections, we can obtain the total reorganization energy for the regeneration reaction as

$$\lambda(r) = \lambda_{porph}^{out}(r) + \lambda_{redox}^{in+out} + \lambda_{porph}^{in} + \lambda_R^{out}(r) \tag{19}$$

where we assume that λ_{porph}^{in} is r independent due to the similarity in chemical structure. The r-independent parts of the above equation are found explicitly from a MD simulation of the diabatic regeneration reaction (eq 1) with the smallest porphyrin in which λ_{redox}^{in+out} have been corrected for the effect of using a finite cell with periodic boundary conditions.

To obtain the electron transfer barrier we need in addition to the reorganization energy also the driving force, ΔF^0, for the regeneration reaction. This quantity is defined as

$$\Delta F^0 = E_{ox}^{porph} - E_{red} \tag{20}$$

where E_{ox}^{porph} is the oxidation potential of the porphyrin dye and E_{red} is the redox potential of the redox mediator. To obtain E_{ox}^{porph} from our calculations we assume that the oxidation potential scales linearly with the vacuum ionization potential calculated from total energy differences, $E_{HOMO} = E_0[N] - E_0[N-1]$, of the dyes with a constant shift due to solvation energies, image charge effects, etc. Fitting our calculations to the experimental oxidation potentials of 5 porphyrin dyes on TiO_2 measured by Liu et al.[7] we obtain the relation

$$E_{ox}^{porph} = E_{HOMO} - 0.11\ \text{eV} \tag{21}$$

We now have ΔF^0 and $\lambda(r)$ for all 5000+ porphyrin dyes, and we can then calculate the barrier height using the Marcus expression (solving for the crossing between initial and final state free energy curves using eq 14)

$$\Delta F^{\ddagger}(\Delta F^0, \lambda) = \frac{(\lambda + \Delta F^0)^2}{4\lambda} \tag{22}$$

DOI: 10.1021/jp512627e
J. Phys. Chem. C 2015, 119, 12792−12800

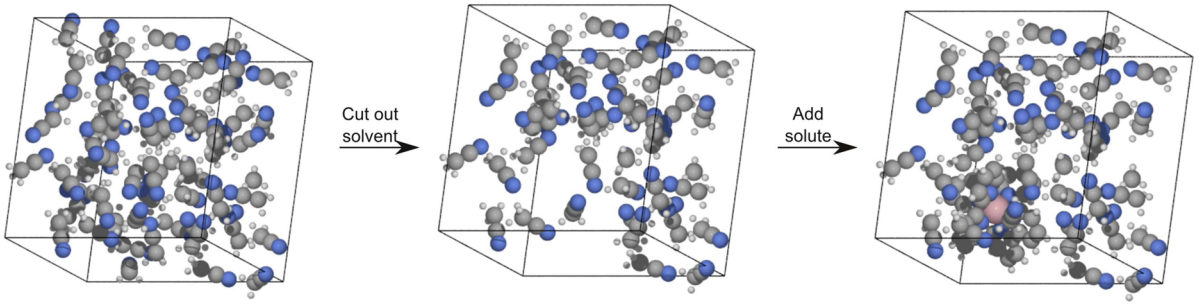

Figure 3. Illustration of the procedure to create the simulation cell for $[Co^{II/III}(bpy)_3]$. A 20 Å × 20 Å × 15 Å unit cell with periodic boundary conditions is filled with acetonitrile and thermalized. After this a hole is cut, and in the last step the desired molecule is inserted.

Weighted Level Alignment Quality. We previously defined the level alignment quality as[16,17]

$$\eta = \frac{eV_{oc}\int_{E_c-E_H}^{\infty}\Theta(E-E_1)\cdot I_{solar}(E)\mathrm{d}E}{\int_0^{\infty}E\cdot I_{solar}(E)\mathrm{d}E} \tag{23}$$

where

$$\Theta(E-E_1) = \begin{cases} 1 & \text{for } -E_1 \geq 0 \\ 0 & \text{for } E-E_1 < 0 \end{cases}$$

Here $E_c - E_H$ is the distance from the HOMO level to the conduction band, E_1 is the optical gap of the dye, $\Theta(E-E_1)$ is a step function representing the absorption of the dye molecules, $I_{solar}(E)$ is the photon flux of the ASTM G-173-03 (AM 1.5 G) solar spectrum, and eV_{oc} is the open-circuit voltage multiplied with the charge of the electron. In the following we assume that $E_c = -4.0$ eV, consistent with using TiO_2 as the semiconductor and $V_{oc} = E_c - E_{red}$. This definition of the level alignment quality neglects all loss mechanisms and only takes the level alignment between semiconductor and the dye molecule into account. An in-depth discussion of the level alignment quality is given in previous publications.[16,17]

Having obtained the regeneration barriers for different dyes and redox mediators it is possible to include this information in a correction factor to correct the level alignment quality. Inspired by the Arrhenius expression we write

$$\eta_{reg}(\Delta F^0, \lambda; T) = C(\Delta F^0, \lambda; T)\cdot\eta \tag{24}$$

where

$$C(\Delta F^0, \lambda; T) = \begin{cases} \exp\left(\dfrac{-\Delta F^{\ddagger}(\Delta F^0, \lambda)}{k_B T}\right) & \text{for } \Delta F^0 \leq 0 \\ 0 & \text{for } \Delta F^0 > 0 \end{cases} \tag{25}$$

We note that the correction function is highly dependent on the used temperature, and this may be important for solar cells, where the working temperature may be very high under intense sunlight. A flowchart illustrating the steps in calculating the weighted level alignment quality is shown in Figure S8, Supporting Information.

Computational Details. All quantum mechanical calculations were performed using density functional theory (DFT)[36] with the PBE[37] exchange-correlation functional as implemented in the GPAW code.[38] For all standard calculations we used a basis set of numerical atomic orbitals[39] (LCAO mode) with a double-ζ polarized basis set, a grid spacing of 0.18 Å, and a 20 Å × 20 Å × 15 Å unit cell with periodic boundary conditions in all directions. To prepare for the molecular dynamics (MD) simulations, the cell was initially filled with acetonitrile to obtain a density of ρ = 786 mg mL^{-1}, which was thermalized to 300 K with 2.0 fs time steps. This is accomplished with an in-house Langevin integrator employing the RATTLE[40] constraint scheme (algorithm based on the formulation by Eijnden et al.[41]). The constraints introduced consist in the pacification of all C−H bonds, which allows us to take larger time steps and thus decrease the computational time required. Since the role of the C−H bonds in the simulations are very limited we believe that the pacification is justified. After the thermalization, a block of solvent molecules was cut out of the unit cell to make room for the dye or redox mediator molecule (see Figure 3 for an illustration of the procedure). Effectively, this gives a conentration of 0.28 M. Since all boxes are similar in size and only contain one solute molecule, the concentration ratio between all species is unity. The solutes are however electrostatically decoupled from the neighboring cell (resulting from the periodic boundary conditions) through the Ewald method. Thus, we are focusing on a single species, corresponding to the infinite dilution limit. The resulting box, containing the solvated molecule, was then thermalized in the same manner as the initial solvent box. To obtain data for the WHAM method (see discussion above) we created five copies of the thermalized box with the solvated molecule and thermalized them using a linear combination of initial and final state forces with χ_α = 0.0, 0.25, 0.50, 0.75, and 1.00 for each box. After 1.0 ps of thermalization we ran the simulation for an additional 5.0 ps production time, resulting in 2500 data points for every configuration. Combining the data point for the WHAM procedure lead to in total 6.25 million data points for every linear force combination.

RESULTS AND DISCUSSION

The values for all explicitly calculated reorganization energies are given in Tables S2 and S3, Supporting Information, and the constructed Marcus parabolas for the regeneration of the simplest zinc porphyrin dye by $^{LS}[Co^{II/III}(bpy)_3]$ are given in Figure 4. Correcting the calculated λ_{PBC} for the symmetric electron transfer between two porphyrins (ZnP + ZnP$^+$ → ZnP$^+$ + ZnP) for the periodic boundary conditions and the screened coulomb interaction (eq 18) we obtain λ = 0.89 eV. This value is in good agreement with the λ = 0.84 eV reported by Osuka et al.[42] for a comparable electron transfer in porphyrin dyads in DMF. Considering the cobalt-based redox mediators, we note that the energy difference between the high-spin (HS) and the low-spin (LS) states of cobalt(II) species is

DOI: 10.1021/jp512627e
J. Phys. Chem. C 2015, 119, 12792−12800

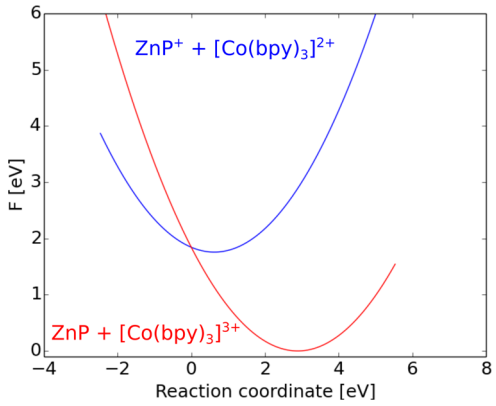

Figure 4. Constructed Marcus parabolas for the regeneration of the simplest zinc porphyrin dye by $^{LS}[Co^{II/III}(bpy)_3]$. The blue curve is $F_i(x)$, and the red curve is $F_f(x)$. ΔF^0 (obtained from eq 21) is −1.76 eV, and the PBC and screened Coulomb interaction-corrected calculated λ is 1.30 eV. Since $-\Delta F^0 > \lambda$ the reaction is predicted to be in the Marcus inverted region.

small.[43] Thus, it may be hard to identify the correct ground spin state using DFT, and we therefore investigated both HS and LS for the two redox mediators in question. In line with previously reported results[44] we here find that the reorganization energy involving the HS is around 1 eV higher than for the LS case. As our calculated and corrected reorganization energies for the regeneration reactions with the LS species resemble the experimental values obtained for the regeneration of an organic dye using different cobalt-based redox mediators reported by Feldt et al.[45,46] we find it likely that these reorganization values give the best representation. We therefore in the following assume that all cobalt species are LS. We further note that our obtained reorganization energies are higher than those recently reported for the cobalt redox mediators using continuum models for the solvent.[44,47] This is expected since we capture the solvent reorientation by including an explicit solvent. Furthermore, we do not include the lowering of the reorganization caused by the immobilization of the dyes introduced by the bonding to the semiconductor. In the following we present the calculated barrier heights associated with the regeneration reaction and the resulting correction function and weighted level alignment quality for all 5000+ porphyrin dyes. It should be noted that in order to obtain high efficiency in a DSSC using cobalt-based redox mediators, it is necessary to have dyes with bulky side groups (e.g., long alkane chains) to prevent electron recombination from TiO_2 to the cobalt species.[14,23] The dyes investigated in this study are however all relatively small due to computational considerations. Using versions with longer alkane chains should not alter the electronic structure of the dyes significantly, and thus, this will only lead to a lowering of the reorganization energy.

Regeneration Barrier Heights. Figure 5 shows the calculated electron transfer barrier (eq 22) as a function of ΔF^0 for all 5000+ porphyrin dyes with both redox mediators. In both figures a clear quadratic dependence on the driving force is observed with minima around $\Delta F^0 = -1.2$ eV for $[Co^{II/III}(bpy)_3]$ and $\Delta F^0 = -1.3$ eV for $[Co^{II/III}(bpy\text{-}pz)_2]$. According to eq 22 the minimum in barrier height is obtained for $\Delta F^0 = -\lambda$, which suggests very high reorganization energies for the regeneration reactions with both redox mediators. In connection with this we note that the deviation from a single parabola for both redox mediators in Figure 5 is negligible. This indicates that the variation in reorganization energy upon functionalizing of the porphyrins is small compared to the total reorganization energy for the regeneration process. Furthermore, the difference in redox potential between the redox mediators (see Table S4, Supporting Information) is clearly observed in the figures as the largest barriers for $[Co^{II/III}(bpy\text{-}pz)_2]$ are obtained for dyes with only a small driving force, while the source of the large barriers for $[Co^{II/III}(bpy)_3]$ can be both a too small and a too large driving force, the latter corresponding to the Marcus inverted region ($-\Delta F^0 > \lambda$).

Weighted Level Alignment Quality. The level alignment quality, η (eq 23), correction factor, $C(\Delta F^0, \lambda; T)$ (eq 25), and weighted level alignment quality, $\eta_{reg} = C(\Delta F^0, \lambda; T)\cdot\eta$, plotted against the driving force, ΔF^0, is shown in Figure 6 for both redox mediators. Here, it is observed that the level alignment quality increases significantly with decreasing driving force. This can be explained by noting that a lowering of the regeneration driving force is equivalent to decreasing the energy difference $E_c - E_H$ in eq 23. At small driving forces the level alignment quality starts to vary more, which can be ascribed to differences in the first excited state, E_1, for the different dyes. Due to the parabolic shape of the Marcus barriers our proposed correction factors are gaussians centered around $-\lambda$ for the regeneration reactions. Thus, multiplying the level alignment qualities and the correction factors results in weighted level alignment qualities peaking around $\Delta F^0 = -\lambda$. The significant dependence on λ and ΔF^0 strongly influences the obtainable weighted level alignment quality for the two different redox mediators. As the $[Co^{II/III}(bpy)_3]$ redox mediator has both a smaller λ and a lower

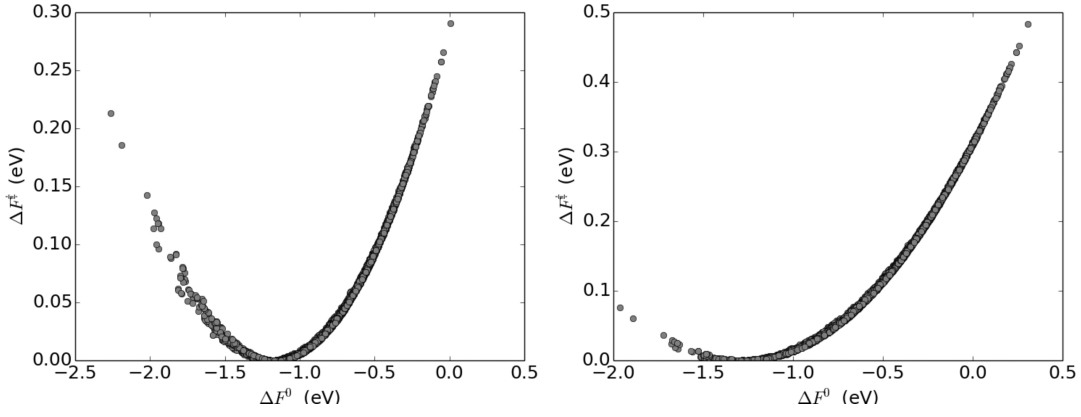

Figure 5. Barrier vs driving force for $[Co^{II/III}(bpy)_3]$ (left) and $[Co^{II/III}(bpy\text{-}pz)_2]$ (right).

DOI: 10.1021/jp512627e
J. Phys. Chem. C 2015, 119, 12792−12800

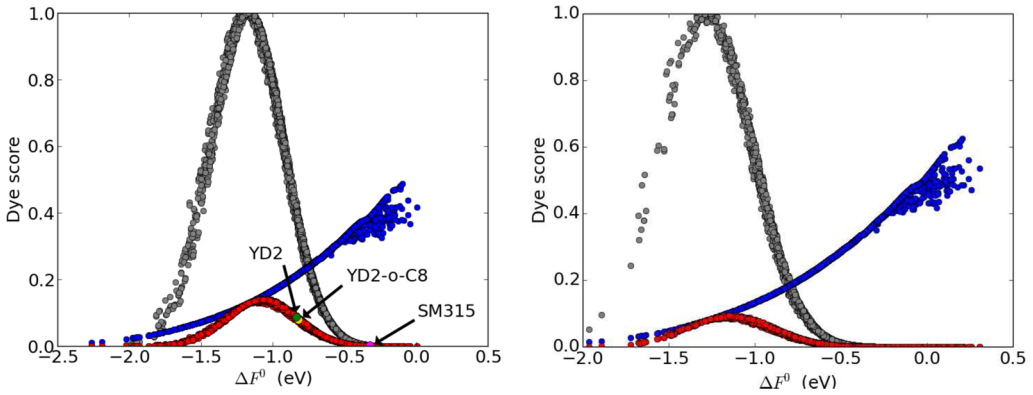

Figure 6. Level alignment quality, η (blue), regeneration correction, $C(\Delta F^0, \lambda)$ (gray), and weighted level alignment quality, $\eta_{reg} = C(\Delta F^0, \lambda; T)\cdot\eta$ (red) for $[Co^{II/III}(bpy)_3]$ (left) and $[Co^{II/III}(bpy\text{-}pz)_2]$ (right) at 298.15 K. For $[Co^{II/III}(bpy)_3]$ the weighted level alignment qualities for the known high-efficiency dyes YD2 (green), YD2-o-C8,[14] (gold) and SM315[15] (magenta) are indicated.

redox potential (higher energy) increasing the driving force of the regeneration reaction we observe significantly higher weighted level alignment qualities using this redox mediator compared to using $[Co^{II/III}(bpy\text{-}pz)_2]$. Here we note that the larger open-circuit voltage obtainable using the latter redox mediator has been taken into account in the level alignment quality, and thus, the V_{oc} is of less importance compared to ΔF^0 and λ.

The top 10 dyes scored on the weighted level alignment quality at room temperature for both redox mediators are given in Tables S5 and S6, Supporting Information. The tables are dominated by dyes having practically no barrier for the regeneration reaction and thus having correction factors very close to unity. This again indicates that the reorganization energy needed for the regeneration reaction overshadows the increase in the level alignment quality obtained by lowering the driving force. In the left part of Figure 6 the calculated weighted level alignment qualities of the known high-efficiency dyes YD2 and YD2-o-C8[14] with the $[Co^{II/III}(bpy)_3]$ redox mediator are indicated. The reported efficiencies for these dyes are 8.4% and 11.9%, respectively,[14] but according to the weighted level alignment quality presented in the figure, the driving force, is slightly too low for these dyes. However, the dyes are still found within our predicted good region of dyes. On the other hand, the record holding SM315[15] dye (reported efficiency of 13.0%) is seen to have even lower weighted level alignment quality due to a very low driving force. As the working temperature of a DSSC can be higher than room temperature due to the exposure to sunlight, we calculated the weighted level alignment for all dyes with both redox mediators at 500 K and presented the top dyes in Tables S7 and S8, Supporting Information. The temperature mainly defines the width of the Gaussian correction function, and thus, dyes with slightly lower regeneration driving force end in the top. The maximum achievable weighted level alignment quality for both redox mediators however only change by 0.01.

The strong dependence of the weighted level alignment quality on the reorganization energy needed for the regeneration reaction inspired us to look at the dependence of η_{reg} on λ for the individual dyes. The results are presented in Figure S9, Supporting Information, for both redox mediators. Here, it is clearly observed that no systematic dependence of η_{reg} on λ can be observed, indicating that it is not the variation in λ for the individual dyes but rather the reorganization energy introduced by the redox mediator which has the greatest impact on the overpotential needed for the regeneration process. In particular, the internal reorganization energy for the two cobalt redox mediators (Table S1, Supporting Information) is a problem which could be expected to be symptomatic for all octahedral transition metal complexes. Using the I^-/I_3^- redox mediator on the other hand introduces significant challenges due to the complicated mechanism for the corresponding regeneration reaction.[48] Thus, the search for new redox mediators with smaller internal reorganization energy and a simple regeneration mechanism must be considered as a very important part of improving the efficiency of DSSCs.

Regeneration versus Recombination. Our definition of the correction factor puts a penalty on all dyes having any barrier associated with the regeneration process. In reality it would however rather be the relationship between the rate of the *regeneration* reaction and the *recombination* reaction (electron transfer from the conduction band of the semiconductor to the oxidized dye) that influences the efficiency. Feldt et al.[45] investigated the regeneration of the organic D35 dye with different cobalt redox mediators and found that a system with λ = 0.8 eV and ΔF^0 = −0.39 eV for the regeneration reaction still had the regeneration reaction dominating over the recombination reaction. Using eq 22, the barrier of this system is $\Delta F^{\ddagger}$ = 0.05 eV. Assuming that regeneration reactions with a barrier equal to or lower than this threshold will be fast enough to dominate over the recombination reaction, we can redefine our correction factor

$$C' = \begin{cases} 1 & \text{for } \Delta F^{\ddagger} \leq 0.05 \text{ eV} \\ \exp\left(\dfrac{-\Delta F^{\ddagger}(\Delta F^0, \lambda) + 0.05 \text{ eV}}{k_B T}\right) & \text{for } F^{\ddagger} > 0.05 \text{ eV} \end{cases} \quad (26)$$

where we still enforce that C' = 0 if $\Delta F^0 > 0$. Using this definition for the $[Co^{II/III}(bpy)_3]$ redox mediator gives the correction factors and weighted level alignment qualities shown in Figure 7. Compared to Figure 6, we here have a large driving force window in which the level alignment quality dominates, shifting the maximum in weighted level alignment quality toward lower driving forces. As indicated in the figure we can further note that we now find the YD2 and YD2-o-C8 dyes within our set of very good candidates, while the record holding SM315 dye still is predicted to have too low driving forces.

A table of the top 10 dyes with this definition of the correction factor can be found in Table S9, Supporting

DOI: 10.1021/jp512627e
J. Phys. Chem. C 2015, 119, 12792−12800

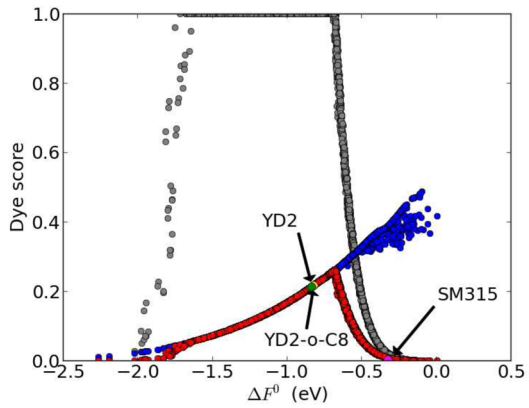

Figure 7. Level alignment quality, η (blue), regeneration correction, $C'(\Delta F^0, \lambda)$ (gray), and weighted level alignment quality, $\eta_{reg} = C'(\Delta F^0, \lambda; T)\cdot\eta$ (red) for $[Co^{II/III}(bpy)_3]$ at 298.15 K using the alternative correction factor C'. The weighted level alignment qualities for the known high-efficiency dyes YD2 (green), YD2-o-C8,[14] (gold) and SM315[15] (magenta) are indicated.

Information. As the table is dominated by dyes having exactly $\Delta F^{\ddagger} = 0.05$ eV, this definition is seen to be extremely sensitive to the chosen threshold value in eq 26, and our choice is thus only one example out of many possibilities. Regardless of the definition of the correction factor, most of the identified top candidates employ a different metal center than the classic zinc center. We therefore believe that our results should encourage exploring, e.g., titanium-based alternatives in the ongoing pursuit for porphyrin-based dyes with high DSSC efficiencies.

CONCLUSIONS

We presented a high-throughput approach to computational design of porphyrin-based dyes for dye-sensitized solar cells. In addition to the energy level alignment and light-harvesting ability of the dyes, the overpotential due to the finite reorganization energy associated with dye regeneration by two commonly used Co redox mediators was taken into account when scoring the dyes. The reorganization energy was calculated using ab initio molecular dynamics for the redox mediators and the simplest Zn−porphyrin dye. These results were then extrapolated to 5000+ functionalized porphyrins using a continuum model for the solvent reorganization energy. We showed that the scheme identifies well-known high-efficiency dyes in addition to a number of new promising candidates. Apart from improving the scoring of the porphyrin dyes, we also identified the reorganization energy of the Co-based redox mediators as an issue to be addressed for improving the efficiency of dye-sensitized solar cells. We propose that new redox mediators with smaller internal reorganization energy than the known octahedral transition metal complexes should be investigated. Here, high-throughput computational methods could be a useful tool.

ASSOCIATED CONTENT

Supporting Information

Derivations, periodic boundary, and finite size corrections; figures with dye backbones, anchor groups, and side groups; tables of explicitly calculated reorganization energies; figures with energy gap distributions and Marcus curves; tables that list of the top 10 dyes based on different scores; figures with weighted level alignment quality as a funtion of the reorganization energy. The Supporting Information is available free of charge on the ACS Publications website at DOI: 10.1021/jp512627e.

AUTHOR INFORMATION

Corresponding Author

*Phone +45 4525 3188. Fax +45 4593 2399. E-mail: thygesen@fysik.dtu.dk.

Present Address

‡Elvar Ö. Jónsson: Department of Applied Physics, Aalto University School of Science, FI-00076 Aalto, Finland.

Notes

The authors declare no competing financial interest.

ACKNOWLEDGMENTS

The authors acknowledge support from the Catalysis for Sustainable Energy (CASE) initiative funded by the Danish Ministry of Science, Technology and Innovation. K.B.Ø. and K.S.T. would further like to thank the Danish Council for Independent Research's DFF-Sapere Aude program (grant no.11-1051390) for financial support.

REFERENCES

(1) Hagfeldt, A.; Boschloo, G.; Sun, L.; Kloo, L.; Pettersson, H. Dye-sensitized solar cells. *Chem. Rev.* **2010**, *110*, 6595−6663.

(2) O'Regan, B.; Grätzel, M. A low-cost, high-efficiency solar cell based on dye-sensitized colloidal TiO_2 films. *Nature* **1991**, *353*, 737−740.

(3) Jung, H. S.; Lee, J.-K. Dye sensitized solar cells for economically viable photovoltaic systems. *J. Phys. Chem. Lett.* **2013**, *4*, 1682−1693.

(4) Li, L.-L.; Diau, E. W.-G. Porphyrin-sensitized solar cells. *Chem. Soc. Rev.* **2013**, *42*, 291−304.

(5) Bessho, T.; Zakeeruddin, S. M.; Yeh, C.-Y.; Diau, E. W.-G.; Grätzel, M. Highly efficient mesoscopic dye-sensitized solar cells based on donor-acceptor-substituted porphyrins. *Angew. Chem., Int. Ed.* **2010**, *49*, 6646−6649.

(6) Moore, G. F.; Konezny, S. J.; Song, H.; Milot, R. L.; Blakemore, J. D.; Lee, M. L.; Batista, V. S.; Schmuttenmaer, C. A.; Crabtree, R. H.; Brudvig, G. W. Bioinspired high-potential porphyrin photoanodes. *J. Phys. Chem. C* **2012**, *116*, 4892−4902.

(7) Liu, B.; Zhu, W.; Wang, Y.; Wu, W.; Li, X.; Chen, B.; Long, Y.-T.; Xie, Y. Modulation of energy levels by donor groups: an effective approach for optimizing the efficiency of zinc-porphyrin based solar cells. *J. Mater. Chem.* **2012**, *22*, 7434−7444.

(8) Masi Reddy, N.; Pan, T.-Y.; Christu Rajan, Y.; Guo, B.-C.; Lan, C.-M.; Wei-Guang Diau, E.; Yeh, C.-Y. Porphyrin sensitizers with [pi]-extended pull units for dye-sensitized solar cells. *Phys. Chem. Chem. Phys.* **2013**, *15*, 8409−8415.

(9) Luo, J.; Xu, M.; Li, R.; Huang, K.-W.; Jiang, C.; Qi, Q.; Zeng, W.; Zhang, J.; Chi, C.; Wang, P.; et al. N-annulated perylene as an efficient electron donor for porphyrin-based dyes: Enhanced light-harvesting ability and high-efficiency Co(II/III)-based dye-sensitized solar cells. *J. Am. Chem. Soc.* **2013**, *136*, 265−272.

(10) He, H.; Gurung, A.; Si, L.; Sykes, A. G. A simple acrylic acid functionalized zinc porphyrin for cost-effective dye-sensitized solar cells. *Chem. Commun.* **2012**, *48*, 7619−7621.

(11) Liu, Y.; Lin, H.; Li, J.; Dy, J. T.; Tamaki, K.; Nakazaki, J.; Nakayama, D.; Nishiyama, C.; Uchida, S.; Kubo, T.; et al. Ethynyl-linked push-pull porphyrin hetero-dimers for near-IR dye-sensitized solar cells: photovoltaic performances versus excited-state dynamics. *Phys. Chem. Chem. Phys.* **2012**, *14*, 16703−16712.

(12) Chaitanya, K.; Ju, X.-H.; Heron, B. M. Theoretical study on the light harvesting efficiency of zinc porphyrin sensitizers for DSSCs. *RSC Adv.* **2014**, *4*, 26621−26634.

(13) Wang, C.-L.; Hu, J.-Y.; Wu, C.-H.; Kuo, H.-H.; Chang, Y.-C.; Lan, Z.-J.; Wu, H.-P.; Wei-Guang Diau, E.; Lin, C.-Y. Highly efficient porphyrin-sensitized solar cells with enhanced light harvesting ability

DOI: 10.1021/jp512627e
J. Phys. Chem. C 2015, 119, 12792−12800

beyond 800 nm and efficiency exceeding 10%. *Energy Environ. Sci.* **2014**, *7*, 1392−1396.
(14) Yella, A.; Lee, H.-W.; Tsao, H. N.; Yi, C.; Chandiran, A. K.; Nazeeruddin, M. K.; Diau, E. W.-G.; Yeh, C.-Y.; Zakeeruddin, S. M.; Grätzel, M. Porphyrin-sensitized solar cells with cobalt (II/III)-based redox electrolyte exceed 12% efficiency. *Science* **2011**, *334*, 629−634.
(15) Mathew, S.; Yella, A.; Gao, P.; Humphry-Baker, R.; Curchod, B. F. E.; Ashari-Astani, N.; Tavernelli, I.; Rothlisberger, U.; Nazeeruddin, M. K.; Grätzel, M. Dye-sensitized solar cells with 13% efficiency achieved through the molecular engineering of porphyrin sensitizers. *Nat. Chem.* **2014**, *6*, 242−247.
(16) Ørnsø, K. B.; Garcia-Lastra, J. M.; Thygesen, K. S. Computational screening of functionalized zinc porphyrins for dye sensitized solar cells. *Phys. Chem. Chem. Phys.* **2013**, *15*, 19478−19486.
(17) Ørnsø, K. B.; Pedersen, C. S.; Garcia-Lastra, J. M.; Thygesen, K. S. Optimizing porphyrins for dye sensitized solar cells using large-scale ab initio calculations. *Phys. Chem. Chem. Phys.* **2014**, *16*, 16246−16254.
(18) Marcus, R. A. On the theory of oxidationreduction reactions involving electron transfer. I. *J. Chem. Phys.* **1956**, *24*, 966−978.
(19) Marcus, R. A. Electrostatic free energy and other properties of states having nonequilibrium polarization. I. *J. Chem. Phys.* **1956**, *24*, 979−989.
(20) Marcus, R. A. On the theory of oxidation-reduction reactions involving electron transfer. II. Applications to data on the rates of isotopic exchange reactions. *J. Chem. Phys.* **1957**, *26*, 867−871.
(21) Marcus, R. A. On the theory of oxidation-reduction reactions involving electron transfer. III. Applications to data on the rates of organic redox reactions. *J. Chem. Phys.* **1957**, *26*, 872−877.
(22) Marcus, R. A. On the theory of electron-transfer reactions. VI. Unified treatment of homogeneous and electrode reactions. *J. Chem. Phys.* **1965**, *43*, 679−701.
(23) Feldt, S. M.; Gibson, E. A.; Gabrielsson, E.; Sun, L.; Boschloo, G.; Hagfeldt, A. Design of organic dyes and cobalt polypyridine redox mediators for high-efficiency dye-sensitized solar cells. *J. Am. Chem. Soc.* **2010**, *132*, 16714−16724.
(24) Yum, J.-H.; Baranoff, E.; Kessler, F.; Moehl, T.; Ahmad, S.; Bessho, T.; Marchioro, A.; Ghadiri, E.; Moser, J.-E.; Yi, C.; et al. A cobalt complex redox shuttle for dye-sensitized solar cells with high open-circuit potentials. *Nat. Commun.* **2012**, *3*, 631−1−8.
(25) Warshel, A. Dynamics of reactions in polar solvents. Semiclassical trajectory studies of electron-transfer and proton-transfer reactions. *J. Phys. Chem.* **1982**, *86*, 2218−2224.
(26) Souaille, M.; Roux, B. Extension to the weighted histogram analysis method: Combining umbrella sampling with free energy calculations. *Comput. Phys. Commun.* **2001**, *135*, 40−57.
(27) Ferrenberg, A. M.; Swendsen, R. H. Optimized Monte Carlo data analysis. *Phys. Rev. Lett.* **1989**, *63*, 1195−1198.
(28) Kumar, S.; Rosenberg, J. M.; Bouzida, D.; Swendsen, R. H.; Kollman, P. A. The weighted histogram analysis method for free-energy calculations on biomolecules. I. The method. *J. Comput. Chem.* **1992**, *13*, 1011−1021.
(29) Tachiya, M. Relation between the electron-transfer rate and the free energy change of reaction. *J. Phys. Chem.* **1989**, *93*, 7050−7052.
(30) King, G.; Warshel, A. Investigation of the free energy functions for electron transfer reactions. *J. Chem. Phys.* **1990**, *93*, 8682−8692.
(31) *Jmol: an open-source Java viewer for chemical structures in 3D*; http://www.jmol.org/, Jmol.org: USA, 2014.
(32) Hummer, G.; García, A. E. Ion sizes and finite-size corrections for ionic-solvation free energies. *J. Chem. Phys.* **1997**, *107*, 9275−9277.
(33) Hünenberger, P. H.; McCammon, J. A. Ewald artifacts in computer simulations of ionic solvation and ionion interaction: A continuum electrostatics study. *J. Chem. Phys.* **1999**, *110*, 1856−1872.
(34) Ayala, R.; Sprik, M. A classical point charge model study of system size dependence of oxidation and reorganization free energies in aqueous solution. *J. Phys. Chem. B* **2008**, *112*, 257−269.
(35) Yaghoobi Nia, N.; Farahani, P.; Sabzyan, H.; Zendehdel, M.; Oftadeh, M. A combined computational and experimental study of the [Co(bpy)3]2+/3+ complexes as one-electron outer-sphere redox couples in dye-sensitized solar cell electrolyte media. *Phys. Chem. Chem. Phys.* **2014**, *16*, 11481−11491.
(36) Kohn, W.; Sham, L. J. Self-consistent equations including exchange and correlation effects. *Phys. Rev.* **1965**, *140*, A1133−A1138.
(37) Perdew, J. P.; Burke, K.; Ernzerhof, M. Generalized Gradient Approximation made simple. *Phys. Rev. Lett.* **1996**, *77*, 3865−3868.
(38) Enkovaara, J.; Rostgaard, C.; Mortensen, J. J.; Chen, J.; Dulak, M.; Ferrighi, L.; Gavnholt, J.; Glinsvad, C.; Haikola, V.; Hansen, H. A.; et al. Electronic structure calculations with GPAW: a real-space implementation of the projector augmented-wave method. *J. Phys.: Condens. Matter* **2010**, *22*, 253202−1−24.
(39) Larsen, A. H.; Vanin, M.; Mortensen, J. J.; Thygesen, K. S.; Jacobsen, K. W. Localized atomic basis set in the projector augmented wave method. *Phys. Rev. B* **2009**, *80*, 195112−1−10.
(40) Andersen, H. C. Rattle: A "velocity" version of the shake algorithm for Molecular Dynamics calculations. *J. Comput. Phys.* **1983**, *54*, 24−34.
(41) V. Eijnden, E.; Ciccotti, G. Second-order integrators for Langevin equations with holonomic constraints. *Chem. Phys. Lett.* **2006**, *429*, 310−316.
(42) Osuka, A.; Noya, G.; Taniguchi, S.; Okada, T.; Nishimura, Y.; Yamazaki, I.; Mataga, N. Energy-gap dependence of photoinduced charge separation and subsequent charge recombination in 1,4-phenylene-bridged zinc-free-base hybrid porphyrins. *Chem.—Eur. J.* **2000**, *6*, 33−46.
(43) Krivokapic, I.; Zerara, M.; Daku, M. L.; Vargas, A.; Enachescu, C.; Ambrus, C.; Tregenna-Piggott, P.; Amstutz, N.; Krausz, E.; Hauser, A. Spin-crossover in cobalt(II) imine complexes. *Coord. Chem. Rev.* **2007**, *251*, 364−378.
(44) Mosconi, E.; Yum, J.-H.; Kessler, F.; Gómez Garcia, C. J.; Zuccaccia, C.; Cinti, A.; Nazeeruddin, M. K.; Grätzel, M.; De Angelis, F. Cobalt electrolyte/dye interactions in dye-sensitized solar cells: A combined computational and experimental study. *J. Am. Chem. Soc.* **2012**, *134*, 19438−19453.
(45) Feldt, S. M.; Wang, G.; Boschloo, G.; Hagfeldt, A. Effects of driving forces for recombination and regeneration on the photovoltaic performance of dye-sensitized solar cells using cobalt polypyridine redox couples. *J. Phys. Chem. C* **2011**, *115*, 21500−21507.
(46) Feldt, S. M.; Lohse, P. W.; Kessler, F.; Nazeeruddin, M. K.; Grätzel, M.; Boschloo, G.; Hagfeldt, A. Regeneration and recombination kinetics in cobalt polypyridine based dye-sensitized solar cells, explained using Marcus theory. *Phys. Chem. Chem. Phys.* **2013**, *15*, 7087−7097.
(47) Sun, Z.-Z.; Zheng, K.-M.; Li, Q.-S.; Li, Z.-S. Rational design of Co-based redox mediators for dye-sensitized solar cells by density functional theory. *RSC Adv.* **2014**, *4*, 31544−31551.
(48) Boschloo, G.; Hagfeldt, A. Characteristics of the iodide/triiodide redox mediator in dye-sensitized solar cells. *Acc. Chem. Res.* **2009**, *42*, 1819−1826.

DOI: 10.1021/jp512627e
J. Phys. Chem. C 2015, 119, 12792−12800